Nanoscale Advances

ROYAL SOCIETY OF CHEMISTRY

COMMUNICATION

View Article Online
View Journal | View Issue

Cite this: *Nanoscale Adv.*, 2021, **3**, 347

Received 27th October 2020
Accepted 28th November 2020

DOI: 10.1039/d0na00900h

rsc.li/nanoscale-advances

Synthesis of Janus Au@BCP nanoparticles *via* UV light-initiated RAFT polymerization-induced self-assembly†

Zhenzhong Liu, [a] Chenglin Wu, [b] Yabo Fu,[b] Xinlei Xu,[a] Jialei Ying,[a] Jiansong Sheng,[a] Youju Huang, *[cd] Chunxin Ma *[ae] and Tao Chen [f]

It is a great challenge to fabricate Janus inorganic/polymeric hybrid nanoparticles with both precisely controlled nanostructures and high yields. Herein, we report a new method to synthesize Janus Au@BCPs *via* UV light-initiated RAFT polymerization-induced self-assembly *in situ* at a high solid content. This strategy provides a promising alternative for achieving asymmetric hybrid nanoparticles with a controllable size, tunable morphology and convenient operation.

Janus inorganic/polymeric hybrid nanoparticles[1,2] are one kind of the most promising nanomaterials and can integrate two or more parts with different chemical/physical properties. In particular, Janus gold nanoparticles/block copolymers (Au@BCPs) have received increasing attention, owing to their potential application in various fields, such as sensors, nanomedicine and catalysis.[3,4] As a type of outstanding polymer ligand to stablize gold nanoparticles (AuNPs), both the architecture and molecular weight of BCPs can be specifically designed and precisely adjusted.[5,6] More importantly, BCP self-assembly is a powerful strategy to fabricate Au@BCP nanoparticles. Based on the technique of concurrent self-assembly,[7,8] AuNPs can be selectively localized well into specific domains of BCP nano-objects (*e.g.*, micelles,[9,10] rods,[11–13] and vesicles[14–16]). However, *via* conventional self-assembly methods, most of the reported Au@BCP nanohybrids are natural symmetric core–shell nanostructures;[17,18] it is still a great challenge to synthesize Janus Au@BCPs with asymmetric nanostructures.

Most recently, a few pioneering studies related to Janus Au@BCP nanoparticles have been developed to achieve asymmetric nanostructures *via* the BCP self-assembly strategy.[19,20] For example, Taton and co-workers[21] fabricated Janus Au@PS-*b*-PAA by the self-assembly of PS-*b*-PAA with AuNPs in dilute solution. Chen's group[22] obtained another Janus Au@PS-*b*-PAA using two ligands to tune the surface energy during hybridization, based on the "mix-and-heat" method. Chen *et al.*[23] further used this method to design more complex Janus Au@BCPs, including gold nanorods, gold nanobipyramids and even gold nanotriangles. However, it is still difficult to massively fabricate Janus Au@BCPs by a facile strategy, which can couple precisely controlled nanostructures and high yields.

In the last several years, polymerization-induced self-assembly (PISA)[24–26] has been explored as an efficient method to design polymeric and inorganic/polymeric hybrid nanoparticles. Different from BCP self-assembly with pre-synthesized polymers, PISA can achieve various controllable morphologies *in situ* at a high solid content during the polymerization process. For example, Bourgeat-Lami *et al.*[27] synthesized multipod-like SiO_2/BCP nanoparticles by nitroxide-mediated PISA. However, as far as we know, the synthesis of Janus Au@BCP nanoparticles directly through the PISA technique has still not been reported, due to the easy aggregation of AuNPs. For example, PISA based on reversible addition fragmentation chain transfer (RAFT),[28–31] which is commonly initiated by heat, easily leads to AuNPs aggregation at high temperature.[32–34] To deal with this problem, in theory, if the PISA process can be initiated by light stimuli (*e.g.*, UV light,[35,36] and vis light[37–40]) at room temperature, more stabilized AuNPs dispersion can be achieved and Janus Au@BCP nanoparticles can be prepared highly efficiently.

Herein, for the first time, we present a new method to synthesize Janus Au@BCP nanoparticles by UV light-initiated

[a]*Research Institute of Zhejiang University-Taizhou, Taizhou 318000, P. R. China. E-mail: chunxinma@zju.edu.cn*

[b]*School of Pharmaceutical and Chemical Engineering, Taizhou University, Taizhou 318000, P. R. China*

[c]*College of Materials, Chemistry and Chemical Engineering, Hangzhou Normal University, Hangzhou 311121, P. R. China. E-mail: yjhuang@hznu.edu.cn*

[d]*National Engineering Research Centre for Advanced Polymer Processing Technology, Zhengzhou University, Zhengzhou 450002, P. R. China*

[e]*State Key Laboratory of Marine Resource Utilization in South China Sea, Hainan University, Haikou 570228, P. R. China*

[f]*Key Laboratory of Marine Materials and Related Technologies, Zhejiang Key Laboratory of Marine Materials and Protective Technologies, Division of Polymer and Composite Materials, Ningbo Institute of Materials Technology & Engineering, Chinese Academy of Sciences, Ningbo 315201, P. R. China*

† Electronic supplementary information (ESI) available: Details of the experimental procedure and analytical data. See DOI: 10.1039/d0na00900h

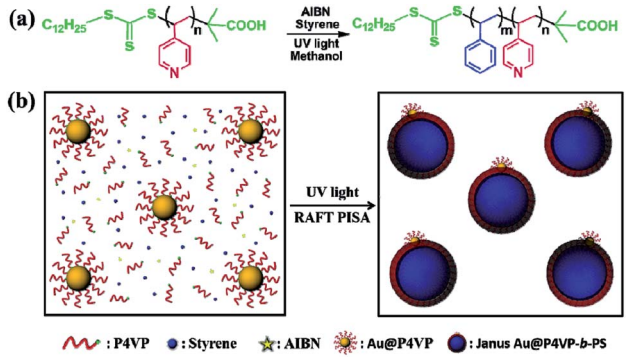

Scheme 1 (a) Synthesis of P4VP-*b*-PS block copolymers. (b) The fabrication of Janus Au@BCP nanoparticles by UV light-initiated RAFT PISA. UV light intensity: $I_{365\ nm} = 2.50$ mW cm^{-2}; irradiation time: 9 h, 25 °C.

RAFT PISA *in situ* at room temperature. The preparation of P4VP-*b*-PS block copolymers and Janus Au@BCPs is shown in Scheme 1. The P4VP chain transfer agent (CTA) was synthesized by thermal-initiated RAFT solution polymerization (Scheme 1a) and the molecular weight was characterized by Gel Permeation Chromatography (GPC) (Fig. S1,† $M_n = 4600$, PDI = 1.23). The AuNPs were prepared by the sodium citrate reduction method and the morphologies were characterized by transmission electron microscopy (TEM) (Fig. S2,† $d = 18 \pm 2$ nm). Then, citrate-capped AuNPs were functionalized with the P4VP-CTA to obtain polymer-tethered Au@P4VP. In a typical process, Au@P4VP was added into methanol solution, which contained the P4VP-CTA chain extender, styrene monomer and 2,2′-azobis(isobutyronitrile) (AIBN) photo-initiator (Scheme 1b). Then the mixture was irradiated under UV light ($\lambda_{max} = 365$ nm, $I_{365\ nm} = 2.50$ mW cm^{-2}, 9 h) at room temperature. When UV light-initiated RAFT PISA was conducted, the P4VP-CTA could initiate styrene to obtain P4VP-*b*-PS block copolymers and spontaneously self-assemble to form micelles localized on the Au@P4VP surface, to achieve Janus Au@P4VP-*b*-PS nanoparticles. Compared with heat-initiated RAFT PISA, this UV light-initiated RAFT PISA can precisely control nanostructures and rapidly fabricate Janus nanoparticles at a high solid content at low temperature.[35] This method can provide a general strategy to fabricate Janus Au@BCPs highly efficiently with controllable asymmetric nanostructures.

Initially, the citrate-capped AuNPs dispersed in water were directly added into a mixture with the molar ratio of P4VP/St/AIBN = 5 : 14 800 : 1 in methanol in UV light-initiated RAFT polymerization (experimental details in the ESI, Table S1†). After 9 h of polymerization, the color of the dispersion changed from pink to milky-red. The original suspension was centrifuged (8000 rpm, 30 min) to separate out the precipitate and redispersed in methanol. The morphologies of the obtained nanoparticles were characterized by TEM. As shown in Fig. S3,† both free P4VP-*b*-PS micelles (without the AuNPs) and Janus Au@BCP nanoparticles (one Au nanoparticle attached with one micelle) were obtained. Why these nanoparticles were directly considered as block copolymer micelles and Au@BCPs nanoparticles here? To confirm this, we will discuss in detail below. It should be noted that a mixture of nanoparticles with a broad size distribution was prepared using the citrate-capped AuNPs, which indicated a loss of control during the PISA process. This is probably because the citrate-capped AuNPs have ligand exchange with the P4VP-CTA (note: as-prepared with an end-capped trithiocarbonate group) through trithiocarbonate interactions[41,42] during photo-polymerization. In order to eliminate the ligand exchange effect and improve the hybridization quality, we assume that the citrate-capped AuNPs can be functionalized with the P4VP-CTA as polymer ligands, which benefits stabilization of AuNPs in organic solvent (*e.g.*, methanol and styrene). Concentrated citrate-capped AuNPs aqueous solution was added into a solution of the P4VP-CTA in methanol and incubated at room temperature. Fig. 1a presents the TEM images of purified polymer-tethered Au@P4VP nanoparticles. The enlarged TEM image in Fig. 1a illustrated the Au@P4VP had a polymer shell about 4 nm on the gold core (marked by red lines and arrows). The surface plasmon resonance (SPR) of the Au nanoparticles can be detected by UV-vis spectroscopy.[21,43] Compared with citrate-capped AuNPs with an absorption peak at 523 nm, that of Au@P4VP had a red shift at 528 nm (Fig. 1b). The surface elemental compositions were further characterized by X-ray photoelectron spectroscopy (XPS). As shown in Fig. 1c, the polymer-tethered Au@P4VP had a distinct peak of N 1s at 398.5 eV, which corresponded to pyridine-like nitrogen in the P4VP-CTA.[44] Finally, the stability of Au@P4VP was examined by UV-vis spectroscopy under UV irradiation. Although the interaction of AuNPs and the trithiocarbonate group of the P4VP-CTA could be destroyed by UV light,[45,46] the results indicated that the curves remain unchanged under irradiation for 4 h in methanol (Fig. S4†). It is important to maintain the stable dispersion of nanoparticles for further polymerization.

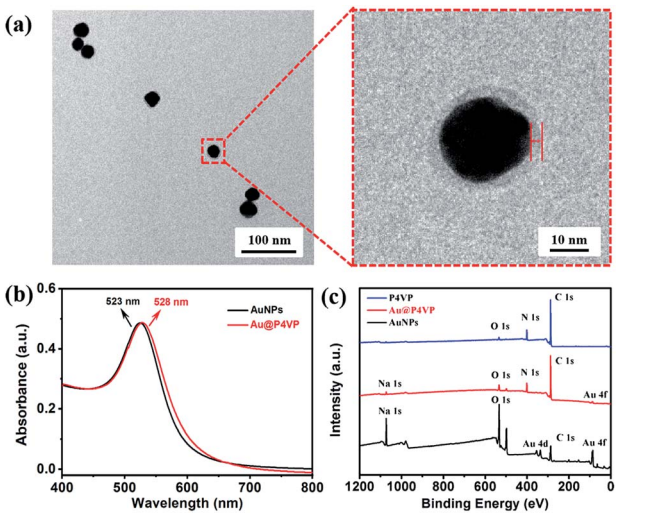

Fig. 1 (a) The large-area (left) and enlarged (right) TEM images of Au@P4VP. (b) The UV-vis spectra of citrate-capped AuNPs and Au@P4VP in methanol. (c) The XPS spectra of the P4VP-CTA, citrate-capped AuNPs and Au@P4VP.

Then, the UV light-initiated RAFT PISA process was carried out in the presence of polymer-tethered Au@P4VP under similar conditions (Table S2†). The recipes of Au@P4VP (200 μL), the P4VP-CTA (4 mg), Styrene (0.1 mL) and AIBN (0.02 mg) in methanol (3.2 mL) were used. After UV irradiation for 9 h, the appearance of the mixture changed from transparent pink to turbid milky-red (Fig. 2a). The obtained nanoparticles were examined by both TEM and scanning electron microscopy (SEM). As shown in Fig. 2a, pure Janus Au@BCPs coupled with precisely controlled nanostructures (the number of Au@P4VP/micelles with the ratio of 1 : 1) were obtained, in which the Au@P4VP part was embedded in the P4VP layer of P4VP-*b*-PS micelles. Moreover, from the large-area TEM image (Fig. S5†) and SEM image (Fig. S6†), the Janus Au@BCP nanoparticles had good controllability and a narrow size distribution. In the UV-vis spectra (Fig. 2b), the SPR band of Janus Au@BCPs changed to 536 nm, which showed about a 8 nm red shift relative to the SPR band of Au@P4VP in methanol (528 nm). This is because the SPR energies decrease as the refractive index of the medium increases.[47,48] In fact, the Janus Au@P4VP-*b*-PS can be destroyed in organic solvents (*e.g.*, THF, and DMF) to obtain the P4VP-*b*-PS block copolymers. Here, the Janus Au@BCP nanoparticles were dissolved in THF and centrifuged (8000 rpm, 30 min) to remove the precipitates. Then, the supernatants were precipitated in *n*-hexane to obtain white solids. After repeated "dissolution-precipitation" for three times and drying under vacuum, the acquired polymers were characterized by ^{1}H NMR spectroscopy and GPC. Compared with the ^{1}H NMR spectrum of the P4VP-CTA in Fig. 2c, the signals assigned to P4VP-*b*-PS (Fig. 2d) were observed and the block ratio of P4VP/PS was 1 : 12, which was calculated based on the integral values of signals at δ = 8.31 ppm (pyridine ring) and δ = 6.57 and 7.09 ppm (phenyl ring). This was also confirmed by the GPC curve in Fig. S7† (M_n = 33 500, PDI = 1.35). Surprisingly, the molecular weight was much higher than that in our previous report.[35] This phenomenon may ascribe to the radical segregation and compartmentalization effect under heterogeneous conditions in RAFT polymerization.[49]

In order to further investigate the formation mechanism of P4VP-*b*-PS micelles on the Au@P4VP surface, both TEM and *in situ* UV-vis spectroscopy were used to monitor the growth kinetics during the UV light-initiated RAFT PISA process. Firstly, the evolution of Janus Au@BCPs was recorded by TEM observation at timed intervals (*e.g.*, 1 h, 3 h, 4 h, 5 h, 7 h and 9 h). As shown in Fig. 3a, a bump about 32 nm formed on the Au@P4VP surface at 3 h. As the polymerization time increased, the size gradually increased to 81 nm (5 h) and finally about 185 nm (9 h) (the large-scale TEM images in Fig. S8†). Previously, Xia *et al.*[50] reported a seed-growth mechanism to prepare Janus Au@PS *via* dispersion polymerization. Notably, our work here is more similar to research on block copolymer micellization on the SiO_2 surface by nitroxide-mediated PISA.[27,51] The evolution of nanoparticles with time was further investigated by *in situ* UV-vis

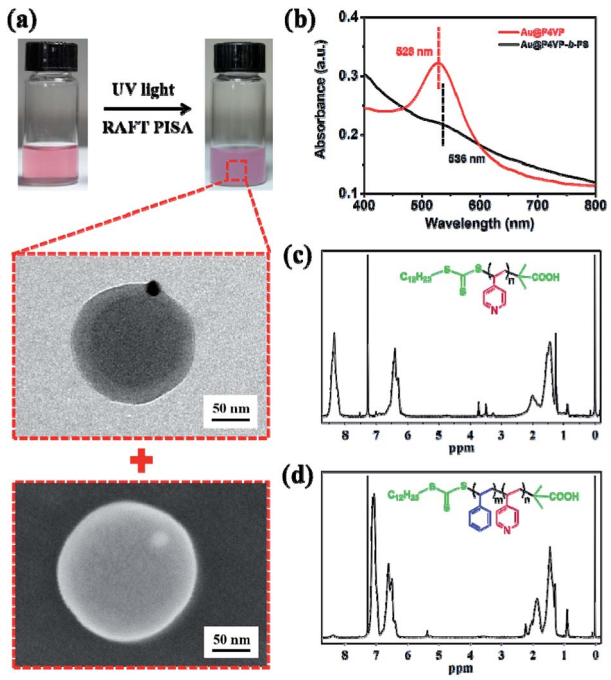

Fig. 2 (a) The optical photographs of the colour change before (left) and after (right) UV light-initiated RAFT PISA. The TEM image (above) and SEM image (below) of a single Janus Au@BCP nanoparticle. (b) The UV-vis spectra of Au@P4VP and Janus Au@BCPs. The ^{1}H NMR spectra of (c) pre-synthesized P4VP-CTA and (d) P4VP-*b*-PS block copolymers purified from Janus Au@BCPs. Experimental conditions: molar ratio of P4VP/St/AIBN = 5 : 14 800 : 1 in methanol. UV light intensity: $I_{365\ nm}$ = 2.50 mW cm^{-2}; irradiation time: 9 h, 25 °C.

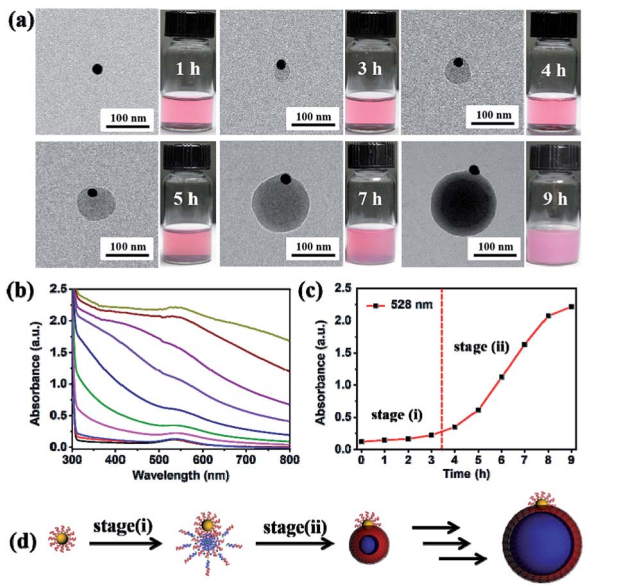

Fig. 3 Kinetics of the growth of Janus Au@BCP nanoparticles *via* UV light-initiated RAFT PISA. (a) Typical TEM images and optical photographs obtained immediately at different times: 1 h, 3 h, 4 h, 5 h, 7 h and 9 h. (b) The UV-vis spectroscopic evolution during polymerization within 9 h. (c) The growth kinetic plot of the peak intensity at 528 nm *versus* the polymerization time. (d) Schematic diagram for the preparation of Janus Au@BCPs *via* UV light-initiated RAFT PISA. Experimental conditions: molar ratio of P4VP/St/AIBN = 5 : 14 800 : 1 in methanol. UV light intensity: $I_{365\ nm}$ = 2.50 mW cm^{-2}; irradiation time: 9 h, 25 °C.

spectroscopy. As shown in Fig. 3b, the absorption curves remain unchanged within 3 h, which were consistent with the optical color change in Fig. 3a. After 3 h, the absorption intensity increased and the characteristic peak gradually shifted from 528 nm to 536 nm. The plot of peak intensity at 528 nm as a function of polymerization time (Fig. 3c) clearly showed that the curves remained almost unvaried within 3 h. Then, the curve quickly increased to a maximum value (9 h), owing to the system that became turbid. The process was also characterized by *in situ* ^{1}H NMR. The results showed that the molecular weight increased with the polymerization time (Fig. S9†). Based on our results, the evolution of Janus Au@BCPs may have two synthetic stages (Fig. 3d): (i) mainly homogeneous polymerization in solution and adsorption on the Au@P4VP surface to form loop micelles. Although there are maybe multiple sites, the fact is that only a single nodule nucleates on the Au@P4VP surface, suggesting that the growing chains can diffuse and coalesce to minimize the interfacial energy.[27] (ii) heterogeneous polymerization in the micelle part to grow into Janus nanoparticles. Polymer chains are initiated in the micelle part and the sizes are determined by the relative amount of the P4VP-CTA and styrene.[52]

Although the synthesis of Janus Au@BCPs has been successfully achieved *via* UV light-initiated RAFT PISA, there still exits some synthetic challenges. It must be pointed out that the hybridization of nanoparticles could be accompanied by free empty micelles (as result of self-micellization).[51] Therefore, we assume that the phenomenon could be avoided by carefully adjusting the recipes in the PISA procedure. In order to confirm our assumption, a series of experiments by tuning Au@P4VP seed, P4VP-CTA and styrene concentrations were conducted in detail (Table S3†). At a high P4VP-CTA and styrene content (entry 1 in Table S3†), a white turbid suspension was obtained after 9 h. As shown in Fig. 4a, it led to a mixture of free P4VP-*b*-PS micelles and Janus Au@BCP nanoparticles. Their size distribution was broad (Fig. 4d) and diameters were from 60 nm to 165 nm (free micelles) and 130 nm to 245 nm (Janus Au@BCPs), respectively. Although free P4VP-*b*-PS micelles accompanied, the pure Janus Au@BCPs strictly complied with the Au@P4VP/micelle ratio of 1 : 1. Based on our proposed mechanism, there is no doubt that when decreasing both the P4VP-CTA and styrene content (entry 2 in Table S3†), the formation of free P4VP-*b*-PS micelles will disappear, leading to pure Janus Au@BCP nanoparticles. Actually, the milky-red suspension was obtained after 9 h, which is consistent with our former phenomenon in Fig. 2a. As illustrated in Fig. 4b, high quality Janus nanoparticles were obtained with almost 100% yields, with an average diameter of 198 nm and a narrow size distribution (Fig. 4e). When we doubled the Au@P4VP content (entry 3 in Table S3†), a deep milky-red suspension was achieved. The results indicated that the average diameter of Janus Au@BCPs narrowed down to 118 nm (Fig. 4c and f), owing to the P4VP-*b*-PS micelle part becoming smaller. Furthermore, these three samples also were characterized by UV-vis spectra analysis (Fig. S10†). As shown in Fig. S10a,† the mixture of Janus Au@P4VP-*b*-PS and P4VP-*b*-PS micelles had no obvious Au specific peak. The bigger Janus Au@BCPs had a clear SPR peak at 536 nm as shown in Fig. S10b.† The smaller one (with a small

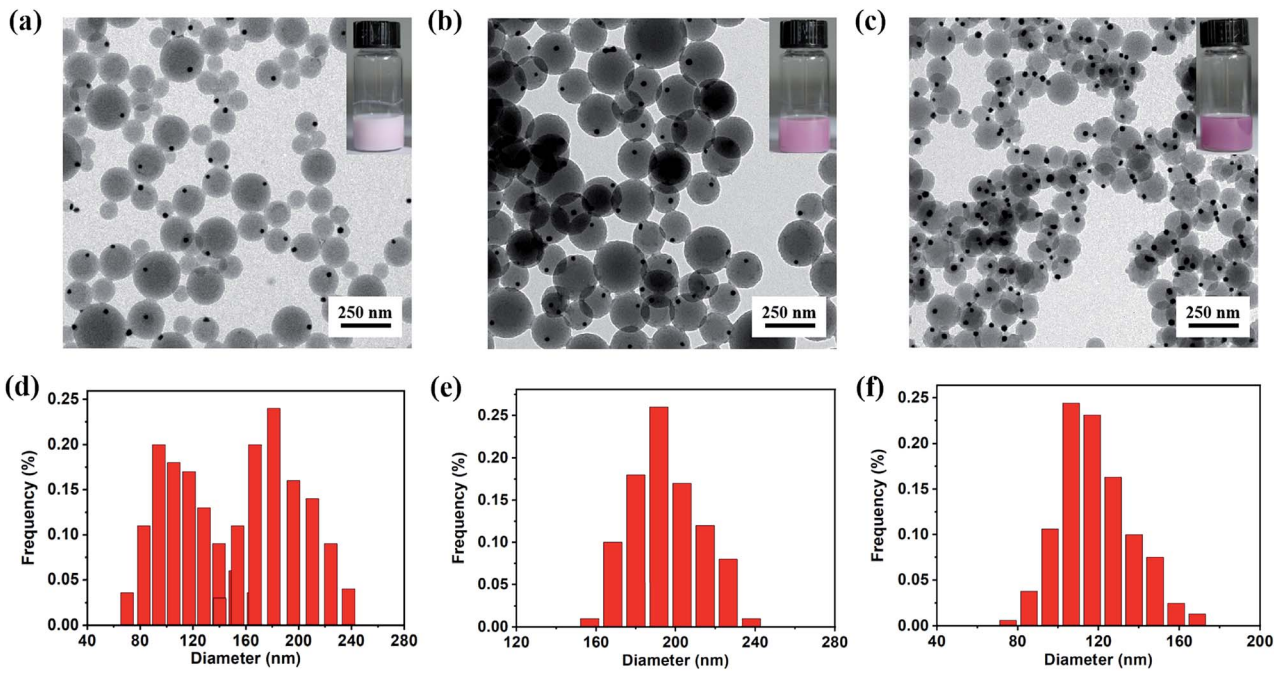

Fig. 4 The TEM images (above) and size histograms (below) of the obtained Janus Au@BCP nanoparticles prepared with different recipes. (a and d) Relatively lower Au@P4VP seed concentration (high P4VP-CTA and styrene contents); (b and e) appropriate Au@P4VP seed concentration; (c and f) relatively higher Au@P4VP seed concentration. Particle size histograms obtained from measurements of at least 150 particles. Inset: the optical photographs of the final dispersion. Experimental conditions: UV light intensity: $I_{365\ nm} = 2.50$ mW cm^{-2}; irradiation time: 9 h, 25 °C.

micelle part) had a stronger intensity with the same SPR peak as shown in Fig. S10c.†

In summary, we have reported a facile method to both massively and controllably fabricate Janus Au@BCP nanoparticles *via* rapidly UV light-initiated RAFT PISA *in situ* at room temperature. The morphology and size of this Janus Au@P4VP-*b*-PS can be precisely tuned by adjusting the recipes and polymerization time. On the one hand, we fixed the recipes to prepare Janus Au@BCPs by *in situ* TEM and UV-vis spectra with the polymerization time. As the polymerization time increased, the size gradually increased at the micelle part of the Janus Au@BCPs. On the other hand, we varied the recipes and fixed the polymerization time, by which the mixture of Janus Au@BCPs and empty micelles, bigger Janus Au@BCPs, and smaller Janus Au@BCPs could be prepared. Polymer-tethered Au@P4VP is the key factor to successfully form Janus Au@BCPs with both controlled quality and high yields. The mechanistic studies revealed that the Janus nanostructures were formed *via* surface-templated self-assembly of block copolymers on Au@P4VP during photo-polymerization. This is the first report on the synthesis of Janus Au@BCP nanoparticles by UV light-initiated RAFT PISA. Compared with traditional concurrent self-assembly in dilute solution, this method is convenient to fabricate hybrid Janus Au@BCPs at a high solid content in one pot at room temperature. This work will provide a general strategy to synthesize asymmetric Janus nanoparticles with a controllable size, tunable morphology and convenient operation. Furthermore, this Janus nanoparticle can also be used as a nano-building block to design and explore hierarchical nanostructures for novel devices.

Conflicts of interest

There are no conflicts to declare.

Acknowledgements

We acknowledge the financial support from the National Natural Science Foundation of China (51873222), Zhejiang Provincial Key R&D Projects (2020C01138), Research Foundations of Hainan University (KYQD(ZR)1814), Taizhou Science and Technology Plan Project (1802GY19 and 1902GY07), and Taizhou-Zhejiang University Science and Technology Program.

Notes and references

1 A. Walther and A. H. E. Muller, *Chem. Rev.*, 2013, **113**, 5194–5261.
2 J. Hu, S. Zhou, Y. Sun, X. Fang and L. Wu, *Chem. Soc. Rev.*, 2012, **41**, 4356–4378.
3 C. Liu, J. Xu and H. Chen, *J. Inorg. Organomet. Polym. Mater.*, 2015, **25**, 153–158.
4 X. Li, H. Yang, L. Xu, X. Fu, H. Guo and X. Zhang, *Macromol. Chem. Phys.*, 2010, **211**, 297–302.
5 J. Du and R. K. O'Reilly, *Chem. Soc. Rev.*, 2011, **40**, 2402–2416.
6 A. H. Groschel and A. H. E. Muller, *Nanoscale*, 2015, **7**, 11841–11876.
7 Y. Mai and A. Eisenberg, *Acc. Chem. Res.*, 2012, **45**, 1657.
8 Y. Liu, B. Liu and Z. Nie, *Nano Today*, 2015, **10**, 278–300.
9 J. Wang, W. Li and J. Zhu, *Polymer*, 2014, **55**, 1079–1096.
10 G. Chen, Y. Wang, L. Tan, M. Yang, L. Tan, Y. Chen and H. Chen, *J. Am. Chem. Soc.*, 2009, **131**, 4218–4219.
11 J. Bae, J. Lawrence, C. Miesch, A. Ribbe, W. Li, T. Emrick, J. Zhu and R. C. Hayward, *Adv. Mater.*, 2012, **24**, 2735–2741.
12 Y. Mai and A. Eisenberg, *Macromolecules*, 2011, **44**, 3179–3183.
13 R. Liang, J. Xu, W. Li, Y. Liao, K. Wang, J. You, J. Zhu and W. Jiang, *Macromolecules*, 2015, **48**, 256–263.
14 Y. Mai and A. Eisenberg, *J. Am. Chem. Soc.*, 2010, **132**, 10078–10084.
15 J. Song, L. Cheng, A. Liu, J. Yin, M. Kuang and H. Duan, *J. Am. Chem. Soc.*, 2011, **133**, 10760–10763.
16 Y. Liu, Y. Li, J. He, K. J. Duelge, Z. Lu and Z. Nie, *J. Am. Chem. Soc.*, 2014, **136**, 2602–2610.
17 H. Wang, L. Chen, Y. Feng and H. Chen, *Acc. Chem. Res.*, 2013, **46**, 1636–1646.
18 Y. Dai and X. Zhang, *Macromol. Mater. Eng.*, 2018, **303**, 1800105.
19 T. Rao, X. Dong, B. C. Katzenmeyer, C. Wesdemiotis, S. Z. D. Cheng and M. L. Becker, *Soft Matter*, 2012, **8**, 2965–2971.
20 X. Song, C. Liu, X. Liu and S. Liu, *ACS Appl. Mater. Interfaces*, 2020, **12**, 3969–3975.
21 Y. Kang and T. A. Taton, *Angew. Chem., Int. Ed.*, 2005, **44**, 409–412.
22 T. Chen, M. Yang, X. Wang, L. Tan and H. Chen, *J. Am. Chem. Soc.*, 2008, **130**, 11858–11859.
23 Z. Wang, B. He, G. Xu, G. Wang, J. Wang, Y. Feng, D. Su, B. Chen, H. Li, Z. Wu, H. Zhang, L. Shao and H. Chen, *Nat. Commun.*, 2018, **9**, 563.
24 J. Sun, C. Hong and C. Pan, *Soft Matter*, 2012, **8**, 7753–7767.
25 N. J. Warren and S. P. Armes, *J. Am. Chem. Soc.*, 2014, **136**, 10174–10185.
26 N. J. W. Penfold, J. Yeow, C. Boyer and S. P. Armes, *ACS Macro Lett.*, 2019, **8**, 1029–1054.
27 X. G. Qiao, P. Y. Dugas, B. Charleux, M. Lansalot and E. Bourgeat-Lami, *Macromolecules*, 2015, **48**, 545–556.
28 R. Bleach, B. Karagoz, S. M. Prakash, T. P. Davis and C. Boyer, *ACS Macro Lett.*, 2014, **3**, 591–596.
29 H. Liu, M. Ding, Z. Ding, C. Gao and W. Zhang, *Polym. Chem.*, 2017, **8**, 3203–3210.
30 M. Tan, Y. Shi, Z. Fu and W. Yang, *Polym. Chem.*, 2018, **9**, 1082–1094.
31 D. Li, X. Chen, M. Zeng, J. Ji, Y. Wang, Z. Yang and J. Yuan, *Chem. Sci.*, 2020, **11**, 2855–2860.
32 W. Huang, G. Skanth, G. L. Baker and M. L. Bruening, *Langmuir*, 2001, **17**, 1731–1736.
33 X. Liu, K. Sun, Z. Wu, J. Lu, B. Song, W. Tong, X. Shi and H. Chen, *Langmuir*, 2012, **28**, 9451–9459.
34 S. Saha, M. L. Bruening and G. L. Baker, *ACS Appl. Mater. Interfaces*, 2011, **3**, 3042–3048.
35 Z. Liu, G. Zhang, W. Lu, Y. Huang, J. Zhang and T. Chen, *Polym. Chem.*, 2015, **6**, 6129–6132.

36 L. Yu, Y. Zhang, X. Dai, L. Zhang and J. Tan, *Chem. Commun.*, 2019, **55**, 7848–7851.
37 J. Tan, Y. Bai, X. Zhang and L. Zhang, *Polym. Chem.*, 2016, **7**, 2372–2380.
38 V. Tkachenko, C. Matei Ghimbeu, C. Vaulot, L. Vidal, J. Poly and A. Chemtob, *Polym. Chem.*, 2019, **10**, 2316–2326.
39 L. Cao, Q. Zhao, Q. Liu, L. Ma, C. Li, X. Wang and Y. Cai, *Macromolecules*, 2020, **53**, 2220–2227.
40 Y. Ma, P. Gao, Y. Ding, L. Huang, L. Wang, X. Lu and Y. Cai, *Macromolecules*, 2019, **52**, 1033–1041.
41 S. Slavin, A. H. Soeriyadi, L. Voorhaar, M. R. Whittaker, C. R. Becer, C. Boyer, T. P. Davis and D. M. Haddleton, *Soft Matter*, 2012, **8**, 118–128.
42 C. Rossner and P. Vana, *Angew. Chem., Int. Ed.*, 2014, **126**, 12849–12852.
43 X. Chen, M. Wei, S. Jiang and S. Förster, *Langmuir*, 2019, **35**, 12130–12138.
44 Z. Sheng, L. Shao, J. Chen, W. Bao, F. Wang and X. Xia, *ACS Nano*, 2011, **5**, 4350–4358.
45 H. Wang, Q. Li, J. Dai, F. Du, H. Zheng and R. Bai, *Macromolecules*, 2013, **46**, 2576–2582.
46 Y. You, C. Hong, R. Bai, C. Pan and J. Wang, *Macromol. Chem. Phys.*, 2002, **203**, 477–483.
47 M. Zhang, N. I. Rabiah, T. H. Ngo, T. P. Otanicar, P. E. Phelan, R. Swaminathan and L. L. Dai, *J. Colloid Interface Sci.*, 2014, **425**, 12–19.
48 J. Song, L. Cheng, A. Liu, J. Yin, M. Kuang and H. Duan, *J. Am. Chem. Soc.*, 2011, **133**, 10760–10763.
49 X. Xiao, S. He, M. Dan, Y. Su, F. Huo and W. Zhang, *J. Polym. Sci., Part A: Polym. Chem.*, 2013, **51**, 3177–3190.
50 A. Ohnuma, E. C. Cho, P. H. C. Camargo, L. Au, B. Ohtani and Y. Xia, *J. Am. Chem. Soc.*, 2009, **131**, 1352–1353.
51 J. Parvole, I. Chaduc, K. Ako, O. Spalla, A. Thill, S. Ravaine, E. Duguet, M. Lansalot and E. Bourgeat-Lami, *Macromolecules*, 2012, **45**, 7009–7018.
52 R. Contreras-Caceres, J. Pacifico, I. Pastoriza-Santos, J. Perez-Juste, A. Fernandez-Barbero and L. M. Liz-Marzan, *Adv. Funct. Mater.*, 2009, **19**, 3070–3076.